



## Evaluation of Lateral and Axial Deformation for Earth Pressure Balance (EPB) Tunnel Construction Using 3-Dimension Finite Element Method

Fahmi Aldiamar<sup>1,\*</sup>, Masyhur Irsyam<sup>2</sup>, Bigman Hutapea<sup>2</sup>, Endra Susila<sup>2</sup> & Ramli Nazir<sup>3</sup>

<sup>1</sup>Institute of Road Engineering, Jalan A.H. Nasution No. 264, Bandung, Indonesia

<sup>2</sup>Faculty of Civil and Environmental Engineering, Bandung Institute of Technology, Jalan Ganesa No. 10, Bandung 40132, Indonesia

<sup>3</sup>School of Civil Engineering, Faculty of Engineering, Universiti Teknologi Malaysia, Malaysia

\*E-mail: fahmi.aldiamar@pu.go.id

### Highlights:

- Surface settlement measurement using surface markers is affected by external factors.
- The soil input parameters should be optimized according stress-strain curve fitting.
- Surface settlement and lateral displacement during TBM construction can be predicted using the hardening soil model (HSM) with 2% contraction.
- The soft soil model (SSM) and the closed-form solutions of Loganathan and Poulos are unable to provide a good displacement result.

**Abstract.** Mass Rapid Transit Jakarta (MRTJ) phase 1 tunnel construction using the earth pressure balance method has been completed and surface settlement and lateral displacement data according to elevation and inclinometer readings has been collected to evaluate the effect of tunnel's construction on surrounding infrastructure. Soil stratification along the research area, defined according to boring logs and soil parameters for the hardening soil model (HSM) and the soft soil model (SSM), was determined by optimization of stress-strain curve fitting between CU triaxial test, consolidation test and soil test models in the Plaxis 3D software. Evaluation of the result of surface settlement measurements using an automatic digital level combined with geodetic GPS for elevation and position control points showed that the displacement behavior was affected by vehicle load and stiffness of the pavement. Lateral displacement measurements using inclinometers give a more accurate result since they are placed on the soil and external influences are smaller than surface settlement measurement. The result of 3D finite element modeling showed that surface settlement and lateral displacement during TBM construction can be predicted using HSM with 2% contraction. SSM and the closed-form solutions of Loganathan and Poulos are unable to provide a good result compared to the actual displacement from measurements.

**Keywords:** *earth pressure balance; finite element method; lateral displacement; surface settlement; tunnel.*

---

Received July 17<sup>th</sup>, 2021, Revised January 6<sup>th</sup>, 2021, Accepted for publication March 18<sup>th</sup>, 2021.  
Copyright ©2021 Published by ITB Institute for Research and Community Services, ISSN: 2337-5779,  
DOI: 10.5614/j.eng.technol.sci.2021.53.5.3

## **1 Introduction**

### **1.1 Background**

Tunnel construction in urban areas is usually conducted using shield tunneling, applying either the earth pressure balance or the slurry method. Both methods are aimed at disturbance reduction at the face of and around the excavation area of the tunnel-boring machine. Although shield tunneling has many advantages, incorrect determination of face loss, shield loss and tail loss could cause settlement or lifting of the ground surface during tunnel construction. Several analytical calculations [1-2], empirical calculations [3-7], and numerical approaches [8-10] for determining surface settlement and lateral displacement have been published in international journals or technical guidelines, i.e. FHWA [11-12], but suitability evaluation based on local ground conditions in Indonesia has not yet been conducted.

Currently, Mass Rapid Transit Jakarta (MRTJ) phase 1 tunnel construction using the earth pressure balance method has been completed. Surface settlement and lateral displacement data according to elevation and inclinometer readings has been collected by Fahmi, *et al.* [13] to evaluate the effect of the tunnel's construction on surrounding infrastructure. This evaluated the relationship between calculated values and measured surface settlement and lateral displacement values to determine which method best represents the actual conditions based on the MRTJ case study. This evaluation also updates the previous publication by Fahmi, *et al.* [13] using different models for ground loss, soil modeling and different soil parameters according to the latest laboratory testing and optimization with the Plaxis 3D soil test utility software.

### **1.2 Research Location**

The twin tube MRTJ tunnel was constructed below existing roads to minimize disturbance of the surface and surrounding activities and also to reduce the need for land acquisition. The tunnel has a diameter of 6.05 m and a lining thickness of 0.25 m, as shown in Figure 1. The construction of both tunnels was conducted sequentially, where tunnel boring machine TBM-1 started first and after around 250 m of advancement TBM-2 was launched.

The research activities were conducted approximately 50 m from the D-wall of Bendungan Hilir Station (Figure 2). Several field tests and laboratory tests were carried out to determine the ground condition and soil properties in this location.

## Evaluation of Lateral and Axial Deformation

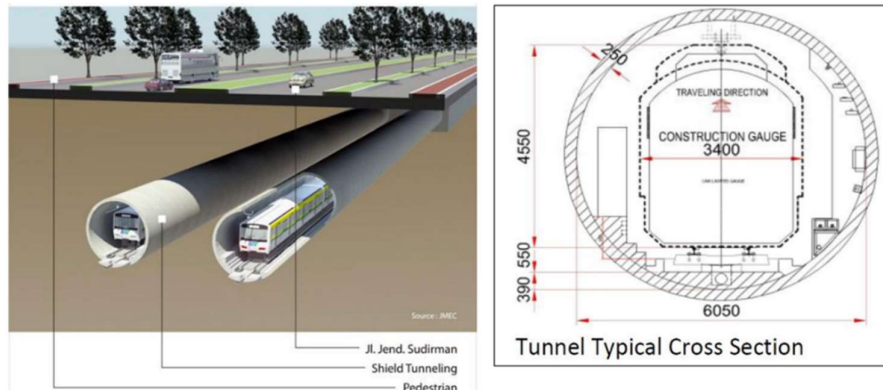


Figure 1 Illustration of MRTJ position and dimensions [14].

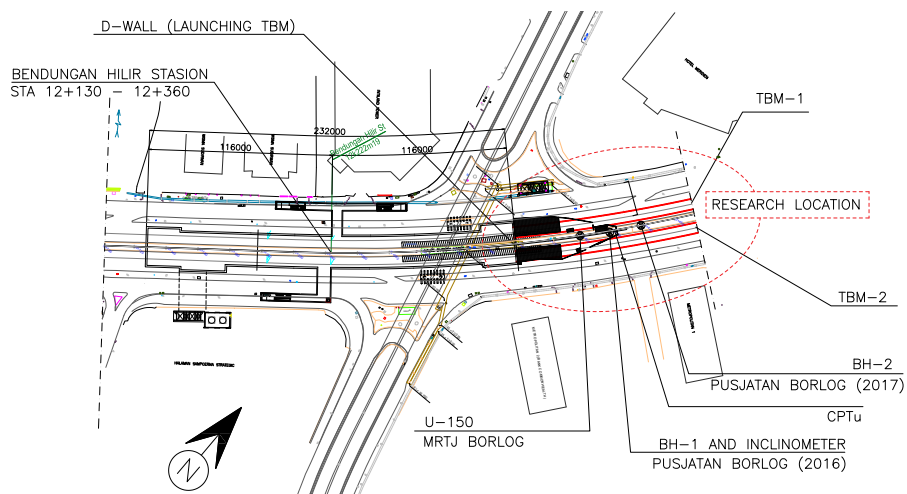
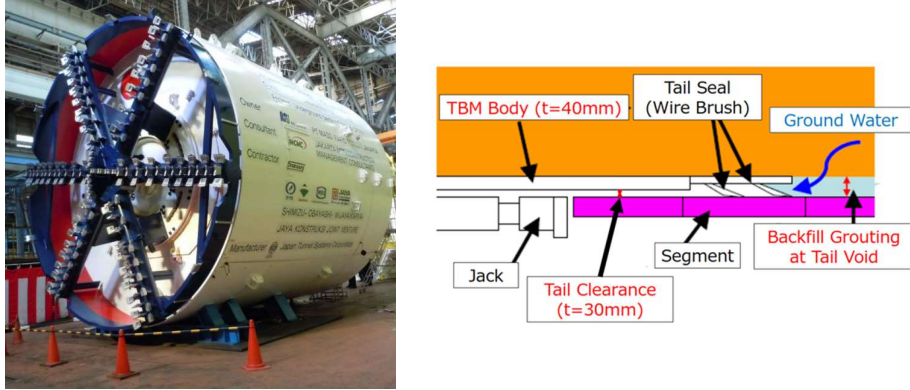


Figure 2 Research location and position of field tests [13].

### 1.3 Earth Pressure Balance (EPB) Tunneling

The earth pressure balance method is based on the equilibrium of earth and water pressure with jacking force applied on the cutter head. A screw conveyor can be used to adjust or control the face pressure during excavation. For tunnels constructed below ground water level, the screw conveyor must be designed to withstand hydrostatic pressure and reduce water pressure to atmospheric pressure. An illustration of the EPB machine used in the MRTJ project is shown in Figure 3(a), while the gap between the TBM body and the lining is shown in

Figure 3(b). The gap between the EPB machine and the lining can cause ground loss and induce displacement around the tunnel construction.



(a) EPB tunneling machine

(b) Shield loss and tail loss at MRT Project

**Figure 3** Illustration of EPB tunnel machine and gap between TBM body and tunnel lining [14].

## 2 Method

### 2.1 Surface Settlement and Lateral Displacement Calculation

Schmidth [15] and Peck [16] were the first to determine the surface settlement curve due to tunnel construction using Eq. (1) and volume of settlement (per unit length of tunnel) using Eq. (2), as shown in Figure 4.

$$S_v(y) = S_{v_{max}} \cdot e^{-\frac{y^2}{2i^2}} \quad (1)$$

$$V_s = \int S_v(y) \cdot dx = \sqrt{2\pi} \cdot i \cdot S_{v_{max}} \quad (2)$$

where:

$S_{v_{max}}$  : settlement above the tunnel axis

$y$  : horizontal distance from the tunnel axis

$i$  : horizontal distance from the tunnel axis to the inflection point of settlement through ground loss

## Evaluation of Lateral and Axial Deformation

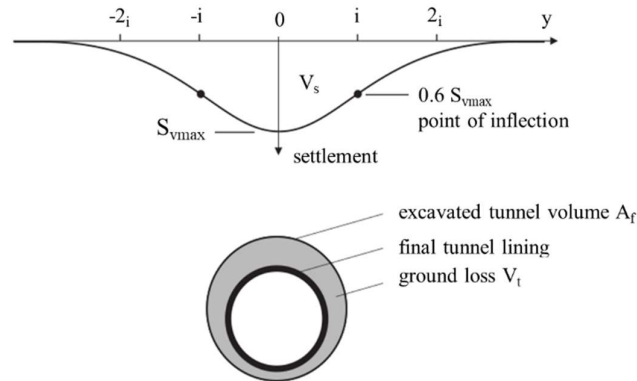


**Figure 4** Gaussian curve for transverse settlement through ground loss [16].

Rowe & Lee in [17] introduced a method for predicting two-dimensional ground loss at the tunnel crown considering ground displacement in the longitudinal and radial directions, as shown in Figure 5, using Eqs. (3) to (5).

$$g = G_p + U^*_{3D} + \omega \quad (3)$$

$$G_p = 2\Delta + \delta \quad (4)$$

$$U^*_{3D} = \left(\frac{k}{2}\right) \delta_x \quad (5)$$

where:

- $G_p$  : physical gap
- $U^*_{3D}$  : three-dimensional elasto-plastic deformation of the tunnel face
- $\omega$  : gap due to the overcutting bead
- $\Delta$  : tunnel lining thickness (m)
- $\delta$  : clearance for erecting the lining (m)
- $k$  : soil-cutter resistance factor
- $\delta_x$  : face intrusion

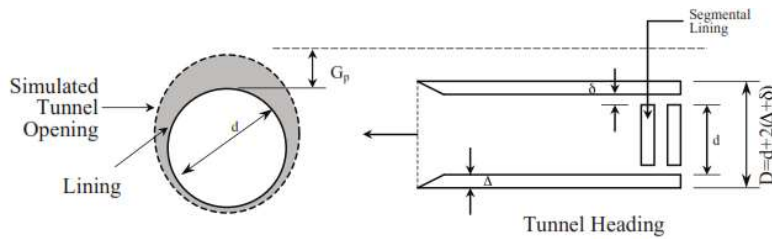


**Figure 5** Physical gap illustration [18].

Verruijt & Booker [1], modified by Loganathan & Poulos [2], describe closed-form solutions for the estimation of settlement and lateral deformation using Eqs. (6) and (7).

$$U_z = -\varepsilon R^2 \left( \frac{z_1}{r_1^2} + \frac{z_2}{r_2^2} \right) + \delta R^2 \left( \frac{z_1(kx^2 - z_2^2)}{r_1^4} + \frac{z_2(kx^2 - z_2^2)}{r_2^4} \right) \quad (6)$$

$$- \frac{2\varepsilon R^2}{m} \left( \frac{(m+1)z_2}{r_2^2} + \frac{mz(x^2 - z_2^2)}{r_2^4} \right) - 2\delta R^2 h \left( \frac{x^2 - z_2^2}{r_2^4} + \frac{m}{m+1} \frac{2zz_2(3x^2 - z_2^2)}{r_2^6} \right)$$

$$U_x = -\varepsilon R^2 \left( \frac{x}{r_1^2} + \frac{x}{r_2^2} \right) + \delta R^2 \left( \frac{z_1(x^2 - kz_1^2)}{r_1^4} + \frac{x(x^2 - kz_2^2)}{r_2^4} \right) \quad (7)$$

$$- \frac{2\varepsilon R^2 x}{m} \left( \frac{1}{r_2^2} + \frac{2mzz_2}{r_2^4} \right) - \frac{4\delta R^2 xh}{m+1} \left( \frac{z_2}{r_2^4} + \frac{mz(x^2 - 3z_2^2)}{r_2^6} \right)$$

where:

- $\varepsilon$  : uniform radial ground loss
- $\delta$  : long-term ground deformation due to ovalization of the tunnel lining
- $z_1$  : z-H
- $z_2$  : x-H
- $r_1^2$  :  $x^2 + z_1^2$
- $r_2^2$  :  $x^2 + z_2^2$
- $R$  and  $h$  : tunnel radius and depth
- $m$  :  $l/(1-2\nu)$
- $k$  :  $\nu/(1-\nu)$
- $\nu$  : Poisson's ratio of soil

## 2.2 Numerical Modeling

3D numerical tunnel modeling was first introduced by Lee & Rowe [19] using a 1-step model, which was further developed into stage construction (step-by-step procedures) by Augarde, *et al.* [20] for circular-shaped tunnels, as shown in Figure 6(a). This model has limitations because it neglects the face pressure, grouting pressure and jacking force acting on the tunnel lining. Hoefsloot & Verwij [21] proposed completed sequence numerical modeling using grouting pressure at the tunnel tail and pressure at the tunnel face, as shown in Figure 6(b). The latest numerical simulation by Litsas, *et al.* [22], as shown in Figure 7, was conducted using the Abaqus software to evaluate the difference between the Modified Cam Clay (MCC) model and the Mohr-Coulomb (MC) model, considering the overcut, face pressure and gap at the TBM tail. This research showed that the MCC model produced larger vertical deformation than the MC model due to the strain-hardening behavior during plastic loading.

## Evaluation of Lateral and Axial Deformation

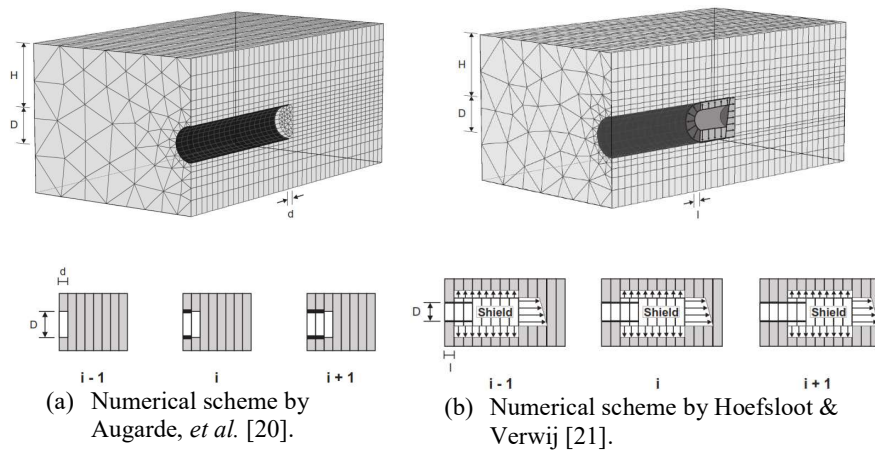


**Figure 6** Stage construction method using numerical modeling.

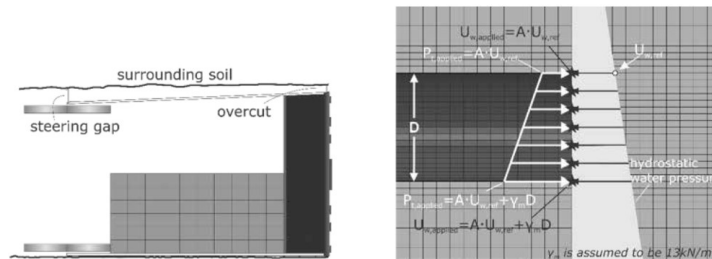


**Figure 7** Numerical model including overcut, tail shield gap and face pressure [22].

In a previous study, Fahmi, *et al.* [13] used MCM, HSM and the soil interface to model ground loss and found that there is different behavior in lateral displacement, especially at the upper part of the soil layer.

This problem may occur due to a lack of accuracy in the soil parameters since the strength and modulus parameters are obtained from correlation. In this paper, improvement of the HSM and SSM parameters was done using laboratory testing and soil test correction. Ground loss was modeled as contraction, which better reflects the actual conditions of TBM excavation in considering the difference in TBM dimensions in the front and tail sections (Figure 8). Variation of TBM contraction was also evaluated to determine a suitable value based on surface settlement and lateral displacement measurements.

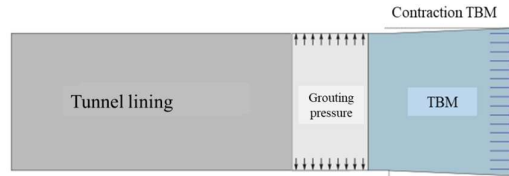


**Figure 8** Numerical model including face pressure, TBM contraction and grouting pressure [23].

### 2.3 Soil Stratification and Parameters

Several soil tests were conducted in the tunnel section at Bendungan Hilir Station for research purposes to obtain an undisturbed sample and develop a longitudinal soil stratification. Based on the soil stratification along the research area, the tunnel construction was predicted through hard silty sand and below ground water level, as mentioned by Fahmi, *et al.* [13] and shown in Figure 9.

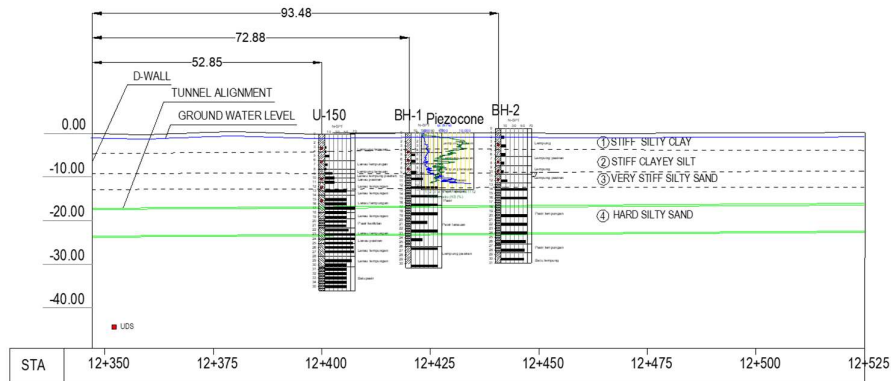


**Figure 9** Soil stratification along the tunnel alignment.

The unloading/reloading Young's modulus,  $E_{ur}^{ref}$ ,  $c'$  and  $\phi'$  as well as the compression index,  $C_c$ , were optimized in this paper based on stress-strain curve fitting between CU triaxial test, consolidation test and soil test models in Plaxis. First, the stress-strain curves from the CU triaxial test samples were plotted and using the best-fit option in Plaxis an approximate curve was plotted, as shown in Figure 10 (a). According to the corrected curve, Mohr circle diagram correction was also determined, as shown in Figure 10(b). The loading-unloading curve to determine Young's Modulus,  $E_{ur}^{ref}$ , was evaluated using the average stress-strain curve resulted from the previous curve fitting, as shown in Figure 10 (c). The same procedure was also conducted to evaluate the consolidation test, as shown in Figure 10 (d).



## Evaluation of Lateral and Axial Deformation

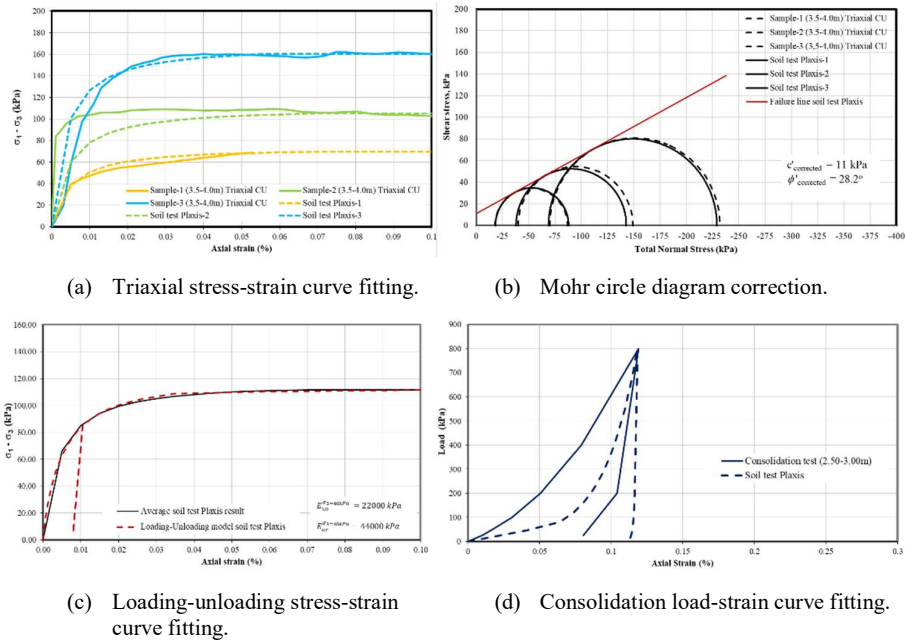


**Figure 10** Example of stress-strain curve fitting using the Plaxis soil test utility.

According to [24], the soil test utility of Plaxis can be used to optimize model parameters such that the best fit is obtained between a model result and a soil lab test result. For SSM, the compression index,  $\lambda$ , is equal to  $C_c/2.303$  and the swelling index,  $K$ , is equal to  $C_s/2.303$ , where the ratios  $C_s/C_c$  or  $K/\lambda$  are about 0.09-0.15 [25].

The pure Poisson's ratio can be assumed to be 0.2 as suggested in the Plaxis manual [23]. Corvello, *et al.* [26] suggested as stiffness parameters for HSM:  $E_{50}^{ref}=1/3 E_{ur}^{ref}$  and  $E_{oed}^{ref}=0.7 E_{50}^{ref}$ . Tables 1 and 2 show a summary of the HSM and SSM soil parameters for numerical modeling according to each soil layer's characteristics.

**Table 1** Hardening soil model (HSM) parameters.

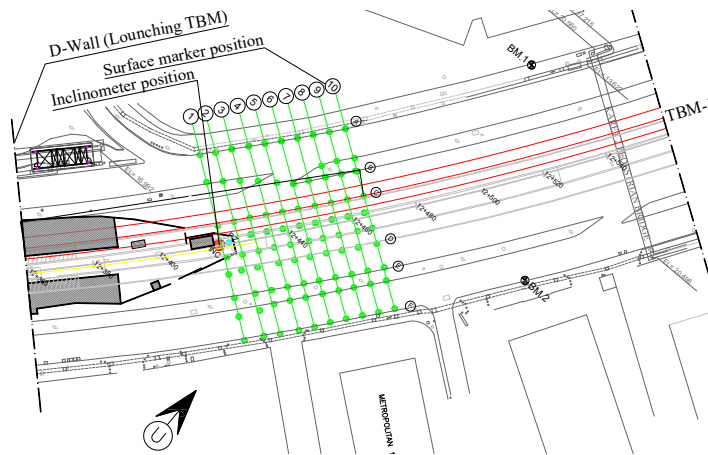
Name	Description	N-SPT (mean)	$\gamma$ (kN/m <sup>3</sup> )	$c'$ (kPa)	$\phi'$ (°)	O C R	Secant stiffness, $E_{50}$ (kPa)	Unload/ reload stiffness, $E_{ur}$ (kPa)	Oedometer stiffness, $E_{oed}$ (kPa)
Layer-1	Stiff silty clay	5	15.48	11	28.2	4.7	22,000	66,000	15,400
Layer-2	Stiff clayey silt	6	15.10	11	28.2	1.8	18,000	54,000	12,600
Layer-3	Very stiff silty sand	11	15.05	13.4	27.7	1.2	19,000	57,000	13,300
Layer-4	Hard silty sand	45	17.00	1	30	1	35,000	105,000	24,500

**Table 2** Soft soil model (SSM) parameters.

Name	Description	N-SPT (mean)	$\gamma$ (kN/m <sup>3</sup> )	$c'$ (kPa)	$\phi'$ (°)	OCR	$\lambda$	K
Layer-1	Stiff silty clay	5	15.48	11	28.2	4.7	0.0233	0.0047
Layer-2	Stiff clayey silt	6	15.10	11	28.2	1.8	0.0210	0.0021
Layer-3	Very stiff silty sand	11	15.05	13.4	27.7	1.2	0.0370	0.0037
Layer-4	Hard silty sand	45	17.00	1	30	1	0.00046	0.000046

## 2.4 Surface Settlement and Lateral Displacement Measurement

The surface elevation measurement data are based on Fahmi, *et al.* [13], conducted using a digital spirit level, while benchmarks for a fixed reference point were placed outside the affected area using a geodetic GPS reference elevation. Surface settlement evaluation was conducted based on 10 cross-section measurements starting at 60 m from the D-wall position (Figure 11).

**Figure 11** Position of surface settlement and lateral displacement measurement.

The spacing of each cross-section was 5 m. Lateral displacement measurement was based on Fahmi, *et al.* [13], conducted using inclinometer instrumentation placed 59.25 m from the D-wall on the right side of TBM-1, around 3.45 m from the outer diameter of TBM (Figure 11). The lateral displacement orientation was perpendicular to the TBM advancement in (A-B) direction and in the TBM longitudinal (C-D) direction. Monitoring of settlement elevation and lateral displacement was conducted from November 21, 2016 until January 9, 2017 in accordance with the TBM-1 construction schedule.

## Evaluation of Lateral and Axial Deformation

TBM-1 had passed all instrumentation points on December 14, 2016 and surface deformation measurement was done on January 9, 2017 as shown in cross-sectional and longitudinal views of the deformation in Figures 12 and 13.

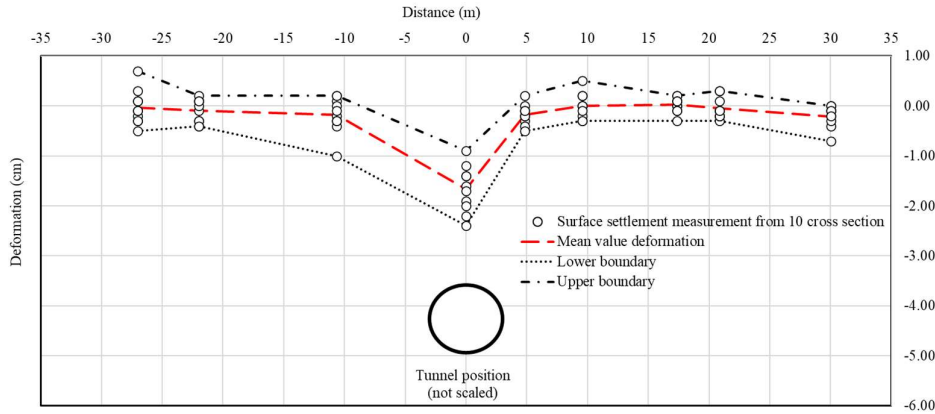


**Figure 12** Cross-sectional view of the deformation after TBM-1 had passed all surface settlement monitoring points [13].

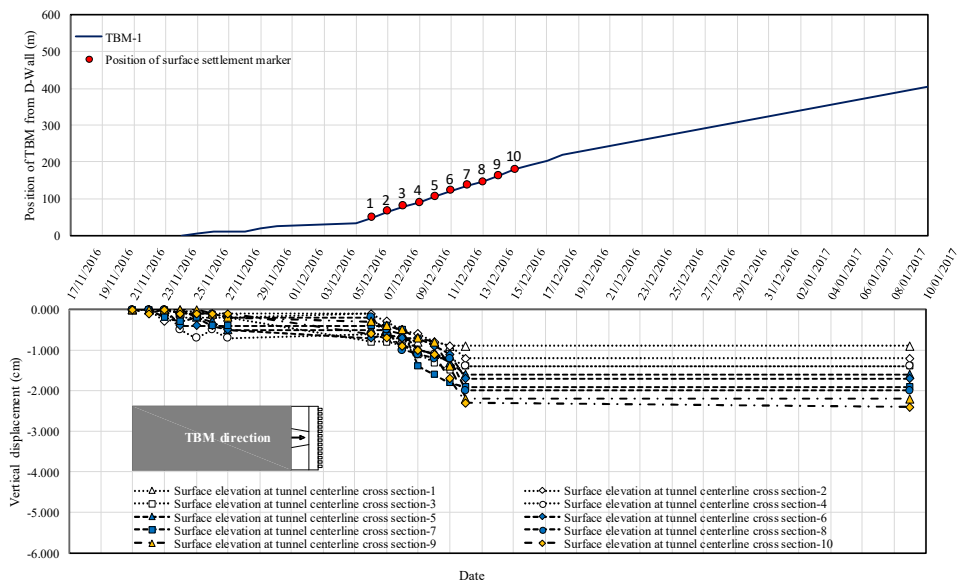
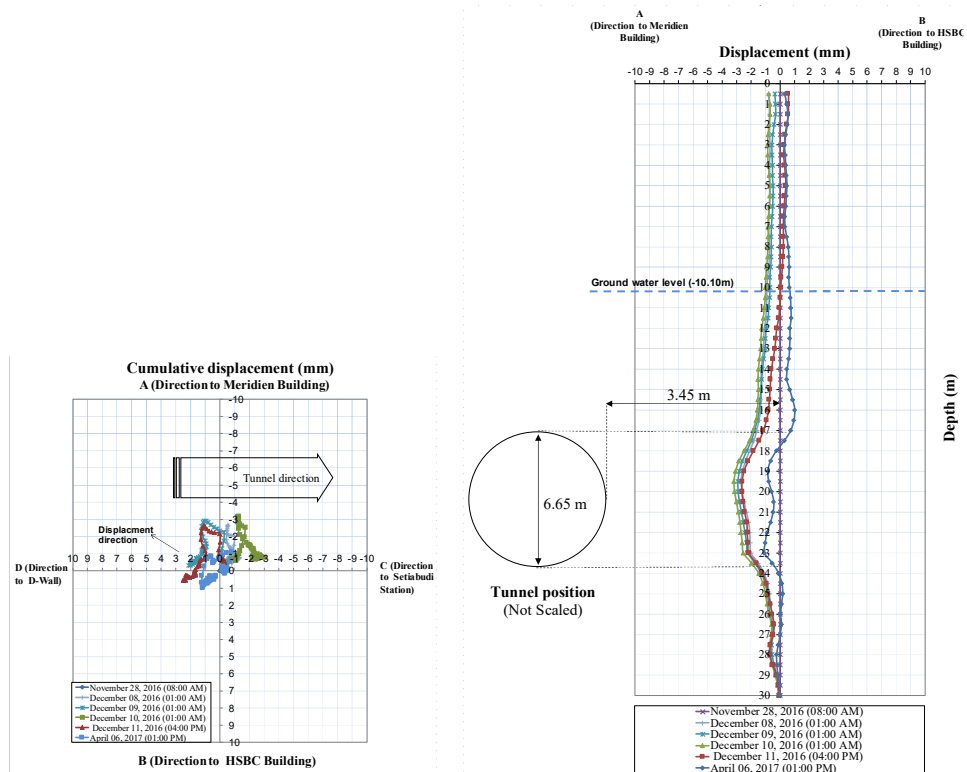


**Figure 13** Longitudinal view of the deformation after TBM-1 had passed all tunnel centerline surface settlement monitoring points.

The longitudinal evaluation of the influence of the tunnel's construction on the inclinometer readings can be seen in Figure 14. The monitoring result shows that all displacement directions lead to the tunnel construction position, especially in the range from 17 m to 23.5 m depth below surface elevation.



(a) Result of top view cumulative displacement.

(b) Result of lateral displacement during tunnel construction.

**Figure 14** Result of inclinometer readings during tunnel construction [13].

The influence of the shield tunnel when passing the inclinometer positions is shown by the ground loss behavior toward the position of tunnel construction and application of grouting, which turns the lateral displacement back to its initial position, as shown in Figure 15.

## Evaluation of Lateral and Axial Deformation

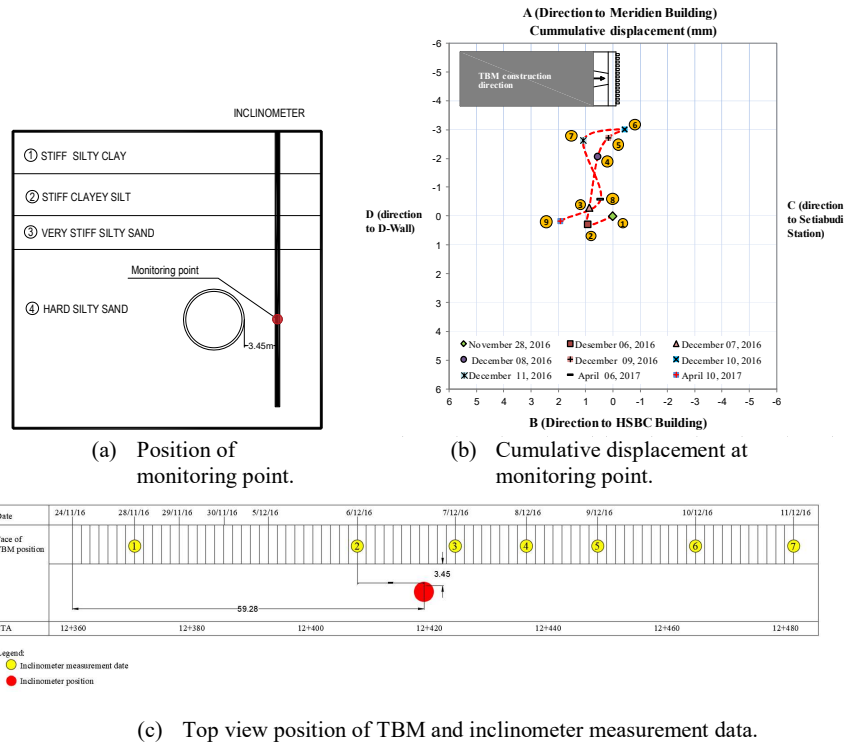


**Figure 15** Cumulative displacement pattern at specific monitoring point.

### 3 Result and Discussion

Evaluation of surface settlement was conducted based on numerical modeling using HSM and SSM parameters (Tables 1 and 2). Variation of the contraction value between 0.5%, 1% and 2.0% of induced vertical deformation was evaluated by comparison with the actual surface elevation. The comparison result between numerical modeling and actual surface settlement when TBM-1 passed the tunnel centerline surface settlement monitoring points in longitudinal view showed that HSM with 0.5% and 1.0% contraction gave a better result than SSM, as can be seen in Figure 16. SSM with 0.5% contraction gave a lower result than HSM, while SSM with 1% and 2% contraction gave a higher result than HSM.

Unfortunately, the thresholds in cross-sectional view are quite different. Since the positions of the surface markers are placed on the road pavement, the displacement was probably affected by vehicle traffic (Figure 17). An overall review of vertical deformation showed that HSM with 0.5% contraction and Peck

in [16] using  $n = 1$  gave the result closest to the actual surface monitoring elevation.

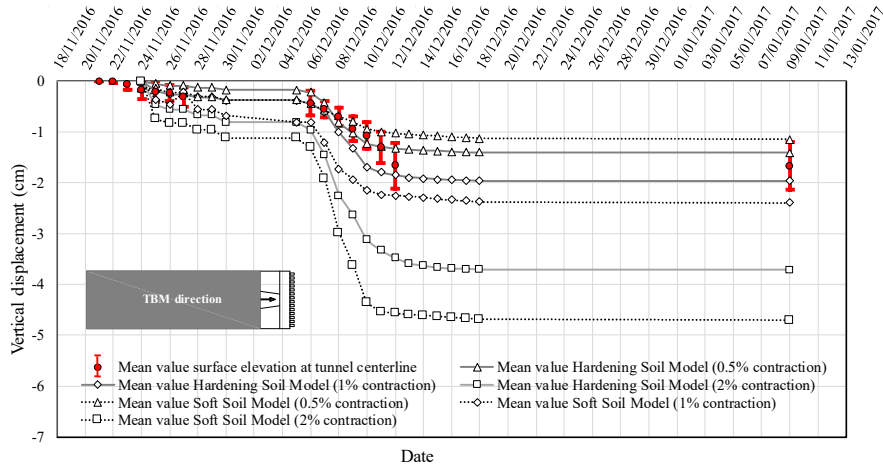


**Figure 16** Comparison between numerical and actual surface settlement in longitudinal view.

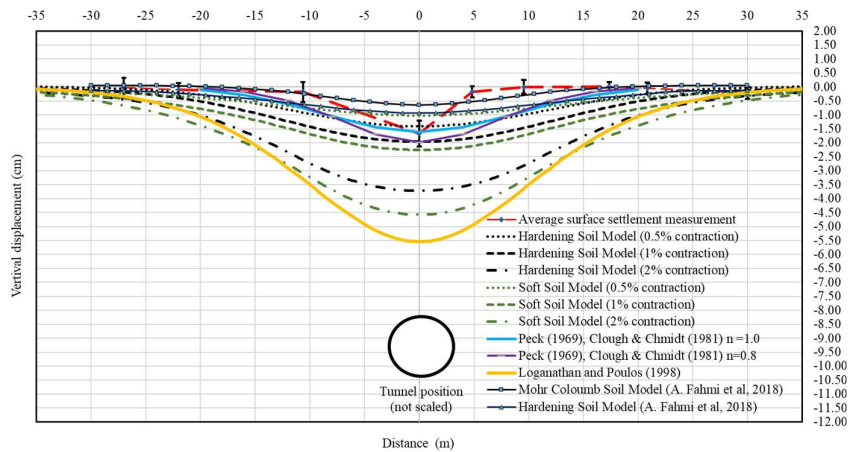


**Figure 17** Comparison between numerical and actual surface settlement in cross-sectional view.

The calculation by Loganathan & Poulos in [2] produced a higher lateral displacement curve than the actual values and those from numerical modeling, as can be seen in Figure 18. Inclinator measurement and numerical modeling using HSM parameters showed better agreement than using SSM, especially at

## Evaluation of Lateral and Axial Deformation

2% contraction, however, the peak lateral displacement curve was higher than the actual inclinometer readings. This contraction value is higher than the result from surface settlement evaluation (1%), however, inclinometer measurement is relatively less influenced by external factors that affect surface settlement, as explained above, so this result is more reliable.

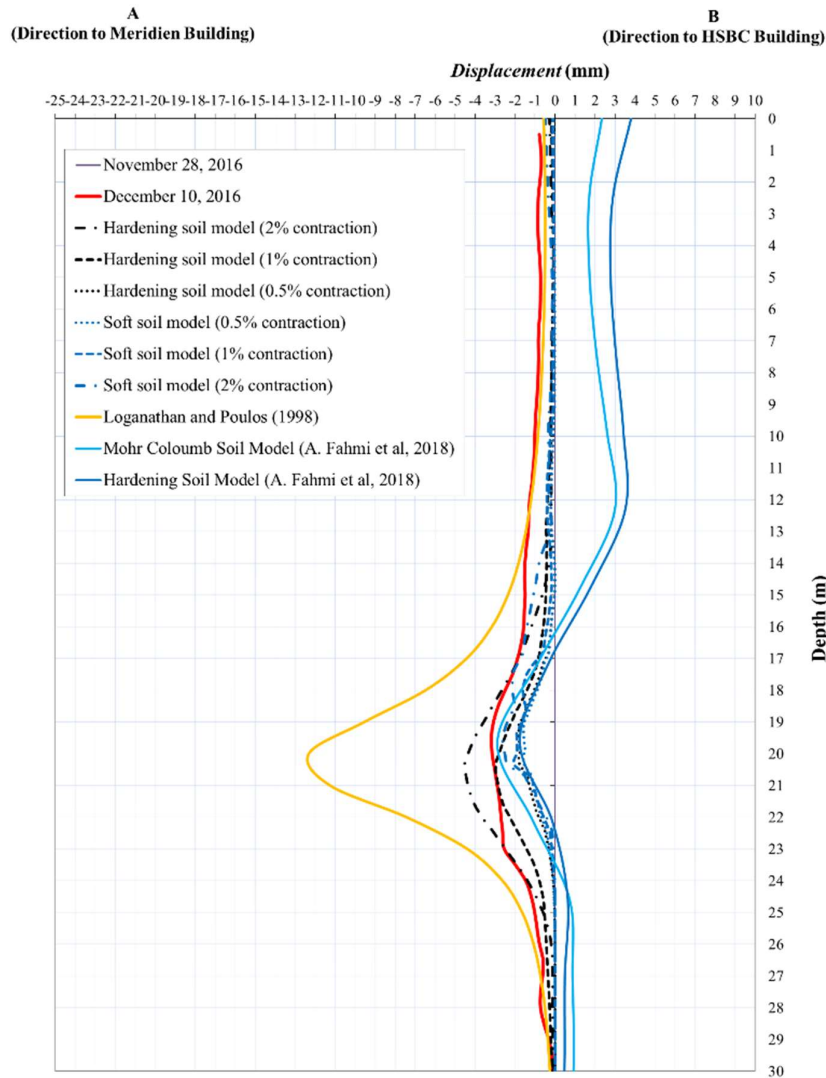


**Figure 18** Comparison between numerical and actual lateral displacement.

#### **4 Conclusion**

Surface settlement measurement using an automatic digital level combined with geodetic GPS for the elevation and position control points produced good displacement data on the surface during tunnel construction. However, since in this project the position of the tunnel was below an existing road and surface settlement markers were mainly placed on the road pavement, displacement behavior could be affected by vehicle load and stiffness of the pavement, leading to inaccuracies. Lateral displacement measurement using inclinometers gives more accurate results and displacement behavior during tunnel construction is also recorded. Since inclinometers are placed on the soil, external influences are smaller than in surface settlement measurement. Soil input parameters should be optimized according to stress-strain curve fitting with the Plaxis soil test utility software to reduce soil disturbances that could occur in soil lab tests.

The contraction model closely resembled the radial soil extension across the tunnel section as soil loosening from ground loss occurred. This phenomenon could be represented by an unload/reload stiffness constitutive model in HSM rather than SSM, which only uses compression stiffness. This is proven by the result of the 3D finite element modeling, which showed the best approximation of surface settlement and lateral displacement during TBM construction using HSM with 2% contraction. The closed-form solution of Loganathan and Poulos mainly depends on prediction of ground loss, which may differ according to the efficiency of the TBM and the soil condition in each country. This approach is a simplified method that usually gives a conservative result compared to numerical modeling.

#### **Acknowledgements**

The author would like to thank the Institute of Road Engineering, Ministry of Public Works; the Research Group of Geotechnical Engineering, Department of Civil Engineering, Faculty of Civil and Environmental Engineering; and the Institute for Research and Community Services (LPPM) of Bandung Institute of Technology.

#### **References**

- [1] Verruijt, A. & Booker, J.R., *Surface Settlements due to Deformation of a Tunnel in an Elastic Half Plane*, *Geotechnique*, **46**(4), pp. 753-756, 1996.
- [2] Loganathan, N. & Poulos, H.G., *Analytical Prediction for Tunneling-induced Ground Movements in Clays*, *Journal of Geotechnical and Geoenvironmental Engineering*, 1998.



## Evaluation of Lateral and Axial Deformation

- [3] Atkinson, J.H. & Potts, D.M., *Stability of a Shallow Circular Tunnel in Cohesionless Soil*, Geotechnique, **27**(2), pp. 203-215, 1977.
- [4] O'Reilly, M.P. & New, B.M., *Settlements Above Tunnels in the UK – Their Magnitude and Prediction*, Tunneling, **82**, pp. 173-181, 1982.
- [5] Mair, R.J., *Developments in Geotechnical Engineering Research, Application to Tunnels and Deep Excavations, Unwin Memorial Lecture*, Proceedings Institution of Civil Engineers, Civil Engineering, **93**, pp. 27-41, 1993.
- [6] Attewell P.B., *Ground Movement Caused by Tunneling in Soil*, Proceeding of the Large Ground Movements and Structures Conference, Cardiff, Pentech Press, London, pp. 812-948, 1977.
- [7] Clough, G.W. & Schmidt, *Excavations and Tunneling*, in *Soft Clay Engineering, Chapter 8*, E.W. Brand & R.P. Brenner, eds., Elsevier, 1981.
- [8] Maji, V.B. & Adugna, A., *Numerical Modelling of Tunneling Induced Ground Deformation and Its Control*, International Journal of Mining and Geo-Engineering, IJMGE, **50**(2), pp. 183-188, 2016.
- [9] Lueprasert, P., Jonpradist, P. & Suwansawat, S., *Tunneling Simulation in Soft Ground Using Shell Elements and Grouting Layer*, International Journal of GEOMATE, **12**(31), pp. 51-57, 2017.
- [10] Litsas, D., Sitarenios, D. & Kavvadas, M., *Advanced Numerical Analysis of EPB Tunneling Using Critical State Plasticity*, World Tunnel Congress, Dubai, UAE, 2018.
- [11] FHWA, *Road Tunnel Design Guidelines*, Federal Highway Administration, US Department of Transportation, Washington DC, 2005.
- [12] FHWA, *Technical Manual for Design and Construction of Road Tunnels*, Federal Highway Administration, US Department of Transportation, Washington DC, 2009.
- [13] Fahmi, A., Desyanti., Masyhur., I., Bigman., H., Endra., S., Riska, M. & Weni, M., *Evaluation of Surface Settlement and Lateral Displacement During Tunnel Construction Using 3D Numerical Modelling*, 20<sup>th</sup> SEAGC-3<sup>rd</sup> AGSSEA Conference Proceedings, Indonesia, 6-7 November 2018.
- [14] Shimizu-Obayashi-Wijaya Karya-Jaya Konstruksi (SOWJ), *Jakarta MRT CP104/105 Construction Progress*, Technical Meeting Material, 2015.
- [15] Schmidt, B.F., *Settlements and Ground Movements Associated with Tunneling in Soils*, PhD thesis, University of Illinois, Urbana, 1969.
- [16] Peck, R.B., *Deep Excavation and Tunneling in Soft Ground*, Proceedings of 7<sup>th</sup> International Conference on Soil Mechanics and Foundation Engineering, Mexico City, State-of-the-art Volume, pp. 225-290, 1969.
- [17] Rowe, R.K. & Lee, K.M., *Subsidence Owing to Tunneling, II Evaluation of a Prediction Technique*, Can. Geotech. J., **29**(6), pp. 941-954, 1992.
- [18] Moller, S., *Tunnel Induced Settlements and Structural Forces in Linings*. PhD thesis. Universität Stuttgart, ISBN-10: 3-921837-54-5, 2006.

- [19] Lee, K.M. & Rowe, R.K., *An Analysis of Three-Dimensional Ground Movements: The Thunder Bay Tunnel*, Canadian Geotech. Jl., **28**, pp. 25-41, 1991.
- [20] Augarde, C.E., Burd, H.J. & Houlsby, G.T., *Some Experiences of Modelling Tunnelling in Soft Ground Using Three-Dimensional Finite Elements*, Proc. 4<sup>th</sup> European Conference on Numerical Methods in Geotechnical Engineering, Udine, 14-16 October, Springer-Verlag, ISBN 3-211-83141-X, pp 603-612, 1998.
- [21] Hoefsloot, F.J.M. & Verweij, A., *4D Grouting Pressure Model Plaxis*, 5th Int. Symposium on Geotechnical Aspects of Underground Construction in Soft Ground, pp. 529-534, 2005
- [22] Litsas, D., Sitarenios, P. & Kavvadas, M., *Advanced Numerical Analyses of EPB Tunneling Using Critical State Plasticity*, ITA-AITES World Tunnel Congress Proceedings, Dubai, 21-26 April 2018.
- [23] Plaxis, *Part 3: Plaxis Material Models Manual*. Delft University of Technology & Plaxis B.V., The Netherlands, 2017.
- [24] Plaxis, *Part 2: Plaxis Reference Manual*. Delft University of Technology & Plaxis B.V., The Netherlands, 2017.
- [25] Lim, A., Ou, C.Y. & Hsieh, P.G., *Evaluation Clay of Constitutive Models for Analysis of Deep Excavation Under Undrained Conditions*, Journal of GeoEngineering, **5**(1), pp. 9-20, April 2010.
- [26] Corvello, M. & Finno, R., *Selecting Parameters to Optimize in Model Calibration by Inverse Analysis*, Computer and Geotechnics, **31**, pp. 410-424, 2004.